The effect of slurry composition on microstructure and mechanical properties of open-cell Inconel foams manufactured by the slurry coating technique

Ninian Sing Kok Ho [a], Peifeng Li [a, *], Srinivasan Raghavan [b], Tao Li [b]

[a] School of Mechanical and Aerospace Engineering, Nanyang Technological University, Singapore

[b] Singapore Institute of Manufacturing Technology, Singapore

[*] Corresponding author's email: peifeng.li@ntu.edu.sg (P. Li); Tel: +65 6790 4766

Abstract

Open-cell nickel-based alloy foams are attractive materials for applications such as sound damping and heat exchange, especially those involving exposure to high temperature environments. This study demonstrated the potential of a developed slurry coating technique for manufacturing open-cell Inconel alloy foams, and then investigated the effect of slurry composition on the microstructure and mechanical properties of the foams. It was found that the compressive properties of the foam can be quantitatively related to its relative density using the empirical equations. The deformation behaviour of the foam is bending-dominated; and unit cell struts undergo brittle fracture after the elastic region. Increasing the slurry solid loading leads to a higher average bulk foam density and more non-uniform crush bands in the foam under compression. Compared to other fabrication processes, this slurry coating technique is able to to produce open-cell Inconel foams with relatively higher strength-to-weight ratios. This study also revealed that the sound absorption capability of the foam increases when its unit cell size is reduced.

Keywords: Foam; Inconel alloy; Slurry coating; Mechanical property; Sound absorption.

1 Introduction

Open-cell metal foams possess a unique combination of properties that make them particularly suitable for a host of applications such as sound damping devices, heat exchangers and catalysts. The existing methods to fabricate such foams can be divided into three categories: solid, liquid and gas state processing. Solid state processing methods involve the use of metal powders and are especially preferred when the alloy of the foam (e.g., Ni) to be produced has a high melting temperature [1]. Among the solid state processing methods, the slurry coating technique can produce open-cell metal foams with the lowest relative densities [2-6]. In this method, an open-cell polymeric sacrificial template is first coated with the metal slurry. The dried slurry-coated template is then subjected to heat treatment to burn off the template and to sinter the metal particles left behind by the slurry. As a result, an open-cell metal foam is produced which takes the shape of the template. The resulting microstructure and mechanical properties of the metal foam are significantly influenced by the slurry composition and the subsequent thermal treatment.

A metal powder slurry for the coating method typically consists of a solvent, a dispersant, a binder and the metal powder itself. To yield successful results, the slurry needs to be both stable and of a suitable viscosity [2]. A stable slurry is homogeneous, which is both “non-agglomerated” and “non-sedimenting”. The viscoelastic slurry serves to contain and transport powdered material during the fabrication process. In a typical metal slurry, the dispersant prevents any flocculation of particles, while the binder increases the viscosity of the slurry, promotes the adhesion during coating and increases the mechanical strength of the unsintered powder. Excess binder may result in flashing, but more importantly causes slumping of parts during debinding. A lack

of binder on the other hand may bring about cracking of parts during debinding. Thus, the powder to binder ratio of a slurry is an important parameter that largely influences its rheological properties and subsequently the outcome of the fabrication process [7]. An optimal range of powder to binder ratios exists for each type of powder. The solid loading of the slurry (Φ), which describes the powder to binder ratio, is closely related to the slurry viscosity and is defined as:

$$\Phi = \frac{\dfrac{W_P}{\rho_P}}{\dfrac{W_P}{\rho_P} + \dfrac{W_B}{\rho_B} + \dfrac{W_D}{\rho_D}} \tag{1}$$

where W_P (ρ_P), W_B (ρ_B) and W_D (ρ_D) are the weight fractions (densities) of the powder, binder and dispersant, respectively. Numerous studies [2, 8, 9] have focused on determining a single optimal slurry composition before using it for foam production. It was found that the viscosity of metal powder slurries (e.g., pure titanium [2], Ti-6Al-4V [8] and aluminium [9]) increases with powder concentration. However, the effect of slurry composition on the resulting foam properties remains largely unknown.

The number of metals that can be used for the slurry coating method remains limited, as fine powders only exist for a small range of metals. Note that the fine metal powders are suggested for the slurry because the use of metal powder particles exceeding 25 μm for the slurry often results in structural defects and voids deep within larger foam pieces [5]. Open-cell foams of stainless steel [5], carbonyl iron [5], Fe-Cr-Al [5, 10], aluminium [9], titanium [2], Ti-6Al-4V [5, 8, 11] and molybdenum [5] have been successfully fabricated using the slurry coating method. However, the production of foams for applications involving exposure to high temperature environments requires that superalloys be used as foam materials. Open-cell foams of Ni-based superalloys have been produced by using various solid state processing

methods, such as the space holder method [12] and electron beam vapour deposition [13]. However, little research reported the use of the slurry coating method for the fabrication of such foams. Queheillalt et al. [6] produced open-cell Inconel 625 foams via a modified slurry coating method whereby binder coated carbon foam templates were suspended in a fluidised airbed to be impregnated by a mixture of Inconel alloy 625 powder and brazing powder before a final heat treatment.

The aim of this study was to develop a novel slurry coating method to produce open-cell Inconel 625 foams, and to investigate the effect of slurry composition on the microstructure, bulk density and mechanical properties of the foam. The effect of unit cell size on sound absorption coefficient was also explored over a selected range of sound frequencies.

2 Experimental procedure

2.1 Slurry coating method to fabricate Inconel foams

Three types of Inconel alloy 625 slurries were prepared as a function of the amount of metal powder to achieve the solid loadings Φ = 0.72, 0.76 and 0.80 (refer to Table 1). The slurry is composed of the Sandvik Osprey (Sandvik Osprey Ltd., UK) 80%–22μm Inconel 625 powder, Butvar B-98 polyvinyl butyral (PVB) (Eastman Chemical Co., TN, USA), stearic acid and ethanol 99.9%, which serve as the metal powder, binder, dispersant and solvent, respectively. After the stearic acid was added to the ethanol, the solution was stirred in an ultrasonic cleaner for 10 min to fully dissolve the stearic acid. The Inconel powder was then poured into the solution, and the mixture was subjected to ball milling for 3.5 hr. The PVB was subsequently added to the mixture that was further ball milled for 19 hr.

Three approximately 20×20×30 mm sacrificial templates were cut from 3M Scotch-Brite commercial dishwashing sponge pads and coated with the three slurries of different solid loadings. Each template was compressed to evacuate as much internal air as possible and then quickly submerged into the slurry, at which point it was allowed to expand to its original shape and size, absorbing the slurry in the process. This technique was observed to facilitate the infiltration of the template by the slurry, reducing the likelihood of incomplete infiltration which causes hollow voids in the resulting Inconel foams. The soaked template was then repeatedly pressed between sheets of absorbent tissue paper to squeeze out the excess slurry until only faint traces of slurry were seen on the paper. Without pressing, the excess slurry would clog the pores of the template and the resulting foam would be partially closed-cell. Finally, the coated template was left to dry overnight in atmospheric air at room temperature.

Subsequently, the dried coated templates were subjected to the heat treatment process in a nitrogen atmosphere in a Carbolite (Carbolite Ltd., UK) furnace. Prior to the heat treatment, thermogravimetric analysis (TGA) in a TA Instruments (TA Instruments Corp., DE, USA) TGA Q500 analyser was conducted on the sponge template material and the slurry components (PVB and stearic acid) to identify the temperature requirements for the heat treatment process. As shown in Fig. 1, these materials started to degrade at different temperatures, and the percentage weight remaining for each tested material was less than 2.0% by 600 °C. Therefore, the thermal profile used during the heat treatment process of the dried coated templates was defined as in Fig. 2. The coated templates were first heated and held at different temperatures (280 °C, 360 °C, 480 °C and 600 °C) to burn off the template and slurry components such as the PVB binder in multiple steps. The metal powders were then

sintered at 1280 °C for 2 hr, and cooled down at 5 °C/min to produce the Inconel foams.

X-ray microtomography (μXT) at 130 kV and 15 μA in a Yxlon (Yxlon Int. GmbH) micro-focus x-ray machine [14-16] was performed on a portion of the 5×5×30 mm specimen cut from the foams. A set of 720 projections was recorded for a full 360° rotation of the specimen in 97 min. After reconstruction, the voxel size in the μXT image was approximately 10 μm. The microstructure of the foams was also examined using a JEOL (JEOL Ltd, Japan) 5600LV scanning electron microscope (SEM) at an accelerating voltage of 15kV.

2.2 Mechanical testing

Cubic specimens with a nominal side length of 5 mm were cut out from the three types of foams using electrical discharge machining (EDM) for compression testing. The side length of 5 mm was chosen to ensure that the specimen size was at least seven times the average unit cell size [17, 18]. Prior to the mechanical tests, all the foam specimens were weighed to obtain their masses. The three dimensions (length, width and height) of each specimen were measured to calculate its volume. The bulk density of the specimen was determined to be the mass divided by the volume [19, 20]. As listed in Table 2, the average bulk density was calculated for the foams with the same slurry solid loading.

Uniaxial compression experiments on the cubic foam specimens were conducted using an INSTRON 5569 mechanical testing machine with a load cell of 500 N capacity. To minimise frictional effects, Castrol LMX grease was applied to the compression platen surfaces that would press against the specimen. The displacement rate was controlled at 0.005 m s^{-1} equivalent to a strain rate of 0.001 s^{-1}. The applied

displacement and resultant force were directly recorded in the INSTRON machine. The compression process of the specimens was captured in a JAI (JAI Ltd., Japan) BM-500 GE high resolution camera. Retests were carried out on the cubic foam specimens until three consistent sets of data (three specimens) were obtained for each type of foam (slurry solid loadings Φ = 0.72, 0.76 and 0.80).

2.3 Acoustic testing

The sound absorption performance of metal foams generally depends on the pore morphology and size [20-22]. Two additional types of open-cell Inconel foams with different controlled porosity were fabricated using the same slurry coating technique for acoustic testing. The slurry solid loading was fixed at Φ = 0.72. The two sacrificial templates used were FoamPartner (FoamPartner Group, Switzerland) Regicell 45 and Regicell 80 reticulated polyester foams with defined and uniform unit cell sizes. Unlike the commercial dishwashing sponges, the unit cell size of the industrial grade Regicell foams was highly controlled with small variations from the nominal value.

A disc-shaped specimen with diameter 30 mm and depth 10 mm was cut from each of the two foams via EDM. The sound absorption coefficient of each specimen was measured at various one-third octave band centre frequencies via the standing wave tube method using the Brüel & Kjær (Brüel & Kjær A/S, Denmark) Standing Wave Apparatus type 4002.

3 Results and discussion

3.1 Microstructure and bulk density

The x-ray microtomographic images (Fig. 3) demonstrate that the Inconel 625 foam with slurry solid loading Φ = 0.76 had an open-cell topology as expected. It would be reasonable to assume that the foam of Φ = 0.72, being less dense, was open-cell as well. Metallographic examinations of the original 20×20×30 mm foam with Φ = 0.80 reveal that the core of the foam was visibly denser than the edges. This indicates that the slurry of Φ = 0.80 was so viscous that the slurry which had penetrated into the core of the template had difficulty in being squeezed out, possibly resulting in closed cells in the core of the foam. Thus for viscous slurries the size and shape of a template influence the bulk density distribution within the final foam product, and the thickest slurry that can coat a template uniformly depends on the pore size of the template. Considering this effect, the cubic foam specimens with Φ = 0.80 were only cut out from the edges of the sintered foam for compression tests and microstructural characterisation.

The SEM examinations (refer to Fig. 4) reveal that in the three types of foams there was excellent bonding between powder particles, and the foam struts had moderately rough surfaces with only occasional powder particles that have not fully bonded into the struts protruding out. An increased metal powder content, all other compositions being kept constant, translates to a greater solid content, which in turn leads to a higher slurry viscosity [9]. A thicker slurry flows out less readily from the sponge template once it has infiltrated the template, depositing more metal powder on the template struts. As observed in the metallographic examinations the wall thickness of the hollow struts in the foams increases with slurry solid loading. Moreover, as the

slurry becomes more viscous (as Φ increases), fewer micro-pores form in the strut walls (Fig. 4), resulting in denser struts. In summary, an increase in slurry solid loading Φ causes a higher average bulk density of the fabricated Inconel foams (refer to Table 2).

3.2 Compressive behaviour

Fig. 5 shows the representative stress–strain curves of the Inconel foams made from the three slurries with different solid loadings. Note that there was good repeatability among the compression tests for each foam type. The curves display similar trends. As in the case of most metal foams [18, 23-25], each stress–strain curve is characterised by three distinct regions, namely the initial linear elasticity, plateau and densification regions (Fig. 5).

All the specimens appeared to undergo largely homogeneous deformation initially, coinciding with the linear elasticity region of their stress–strain curves. Minute inhomogeneity at this point is attributed to the localised plasticity present within the foam even at the bulk stress levels below their peak stresses. As shown in Fig. 6(a), the foam specimen with Φ = 0.72 then developed an approximately horizontal crush band that spread to the rest of the specimen as the compression test progressed. Note that the crush band was identified by tracking the recorded image sequence. However, for the foams with higher Φ = 0.76 and 0.80 (Fig. 6(b) and (c)), the crush band that formed in each specimen was more complicated, often changing in orientation and shape as the specimen was compressed. Furthermore, the crush band also spread outwards to the unaffected portions of the specimen. Although all the crush bands were not exactly planar, the bands in specimens with Φ = 0.76 and 0.80 were much more irregular and random in shape than those in the Φ = 0.72 foam

specimens (Fig. 6). These findings agree with the compressive behaviour of open-cell Duocel aluminium foams as reported in the literature [26]. Density variations were present in every specimen due to the slurry coating method and the stochastic unit cell nature of Scotch-Brite sponge templates, which can cause the complicated shapes of the crush bands. As the solid loading of a slurry increases, the variation in foam density increases and thus the crush bands appear more random and non-uniform.

The open-cell Inconel foam is considered to have a considerably low relative density of less than 0.1 (Table 2), and its unit cell can be approximated by space-filling shapes. The foam is thus expected to be a bending-dominated cellular structure. In the plateau region of the compression, fragments and thus struts broke off and separated totally from the specimens as observed in images captured during the deformation process (Fig. 6). The fragmentation suggests that the Inconel foam is an elastic-brittle foam which undergoes brittle fracture after the linear elasticity region instead of plastic yielding. Therefore, in the typical stress–strain curve of the elastic-brittle Inconel foam, the stress drops sharply immediately after the peak stress is reached and then fluctuates significantly in the plateau region as shown in Fig. 5. This is apparently different from the curve in an elastic-plastic metal foam in which no drop in stress occurs after the compressive strength and a mostly flat plateau region follows.

3.3 Quantitative relation between relative density and mechanical properties

A relationship was established between the slurry metal powder content and the Inconel foam bulk density (Table 2). The compressive properties were subsequently analysed without reference to their slurry Φ values and solely based on their bulk

density (ρ). The Young's modulus E, peak stress σ_{pk} and plateau stress σ_{pl} of metal foams can be quantitatively related to the relative density ρ/ρ_s by the following three equations [27]:

$$\frac{E}{E_s} = C_1 \left(\frac{\rho}{\rho_s} \right)^{\alpha} \tag{2}$$

$$\frac{\sigma_{pk}}{\sigma_{ys}} = C_2 \left(\frac{\rho}{\rho_s} \right)^{\beta} \tag{3}$$

$$\frac{\sigma_{pl}}{\sigma_{ys}} = C_3 \left(\frac{\rho}{\rho_s} \right)^{\gamma} \tag{4}$$

where ρ_s, E_s and σ_{ys} are the density, Young's modulus and yield strength of the strut (solid) material respectively, and C_1, C_2, C_3, α, β, and γ are constants that can be determined experimentally. The α, β, and γ values are dependent on the unit cell topology (connectivity) and the wall material failure mode (brittle or ductile) [27]. For instance, $\alpha = \beta = \gamma = 1.0$ for ideal stretch-dominated cellular structures while $\alpha = 2.0$ and $\beta = \gamma = 1.5$ for ideal bending-dominated structures.

As shown in Figs. 7, 8 and 9, the relative Young's modulus E/E_s, relative peak stress σ_{pk}/σ_{ys} and relative plateau stress σ_{pl}/σ_{ys} of all the tested Inconel foam specimens were regressed against their relative densities ρ/ρ_s in a logarithmic form, taking ρ_s = 8440 kg m^{-3}, E_s = 208 GPa and σ_{ys} = 414 MPa. A good fit was achieved as indicated by the high correlation coefficient $R^2 > 0.96$. The foam is a bending-dominated cellular structure as $\beta = 1.4$ and $\gamma = 1.6$, both of which are close to 1.5. However, $\alpha = 1.3$, which deviates from the expected value of 2.0. The α values other than 2.0 have been found to best fit the results of several open-cell metal foams. For instance, E/E_s was found to increase linearly with ρ/ρ_s for open-cell Duocel aluminium foams over a small range of ρ/ρ_s (0.07 to 0.09) [26]. Moreover, the slope of unloading curves has

been suggested for the determination of E in Eq. 2 due to the presence of localised plasticity, instead of the slope of the loading curve which was used in the present study.

The average peak stress of Inconel foams is higher than that of the other open-cell nickel-based foams of similar relative density which were fabricated by the different foaming processes such as the space holder method [12], slurry coating of carbon foams [6], chromium deposition on Ni foams [28], and electron beam vapour deposition [13] (see Fig. 8). Note that while the foam produced by the electron beam vapour deposition technique [13] has a comparable peak strength, its fabrication cost is also higher. The comparison with other fabrication processes demonstrates the potential of this slurry coating technique to produce low cost Inconel foams with relatively higher strength-to-weight ratios.

3.4 Effect of unit cell size on sound absorption properties

Fig. 10 shows the microstructure of the two Inconel foams fabricated using the Regicell 45 and Regicell 80 foams as sacrificial templates. The pores per linear inch (PPI) in the two templates are PPI = 40–50 and 75–90 respectively, and the two corresponding Inconel foams had nominal unit cell sizes of approximately 508–635 μm (fabricated from template Regicell 45) and 282–339 μm (Regicell 80). The relative densities of the foams were also measured to be 0.039 and 0.052 respectively.

The sound absorption coefficient of the two Inconel foams with different unit cell sizes was measured at various one-third octave band centre frequencies between 800 Hz and 6300 Hz. Fig. 11 illustrates the absorption coefficient versus frequency curves for both foams. At almost all the frequencies used in the acoustic tests, a reduced unit cell size improves the sound absorption performance of the open-cell

Inconel foam. The sound absorption capability is minimal at lower sound frequencies, but becomes effective at frequencies >2000 Hz with a rather narrow peak width. The coefficient curves for the two foams peak at different frequencies of 2500 Hz (unit cell sizes 282–339 μm) and 3150 Hz (508–635 μm). These observations agree with the findings on the sound absorption behaviour of open-cell aluminium foams by Han et al. [20]. The topology of the Inconel foams with a unit cell size of 282–339 μm and a relative density of 0.052 is likely to be equivalent to that of the aluminium foam with a documented cell size 500 μm and a relative density 0.043, as the peaks for sound coefficient occur at around 2500 Hz for both cases.

One possible way to enhance the sound absorption performance of the open-cell Inconel foam would be to reduce its unit cell size by using an appropriate sacrificial template. Furthermore, it would be beneficial, if permissible, to allow for an air gap directly behind the foam that is backed by a rigid plate. This configuration can enhance the sound absorption capability of the foam by shifting the coefficient peak downwards to lower frequencies as well as widening the peak width, as a result of Helmholtz resonant absorption [20, 22].

4 Conclusions

A slurry coating method was developed to fabricate open-cell Inconel 625 foams using slurries of varying composition/solid loading. X-ray microtomography revealed that the topology of the foam was open-cell in nature. The sound absorption capability of the foam improved as the unit cell size decreased, especially at higher sound frequencies. The average bulk density of the foam increased with the solid loading of the slurry. The Young's modulus, peak stress and plateau stress of the foam subjected to uniaxial compression were quantitatively related to the relative density using

empirical equations. The compressive behaviour of the open-cell Inconel foam was bending-dominated. The struts in the foams underwent brittle fracture instead of plastic yielding beyond the linear elasticity region. The increased solid loading of the slurry resulted in more random and non-uniform crush bands in the foam under compression probably due to the variation in local density. It was also found that the average peak strength was higher than that of open-cell nickel-based foams fabricated by other processes in the literature. This comparison suggests that the developed slurry coating technique has the potential to produce open-cell Inconel foams with higher strength-to-weight ratios.

Acknowledgements

The authors gratefully acknowledge the financial support of Academic Research Fund (AcRF) Tier 1 by Ministry of Education, Singapore. N.S.K. Ho also thanks the support of the C.N. Yang Scholars Programme at Nanyang Technological University.

References

[1] A. Kennedy, Porous metals and metal foams made from powders, in: K. Kondoh (Ed.) Powder Metallurgy, InTech, 2012, pp. 31-46.

[2] A. Manonukul, M. Tange, P. Srikudvien, N. Denmud, P. Wattanapornphan, Rheological properties of commercially pure titanium slurry for metallic foam production using replica impregnation method, Powder Technol., 266 (2014) 129-134.

[3] H.I. Bakan, K. Korkmaz, Synthesis and properties of metal matrix composite foams based on austenitic stainless steels -titanium carbonitrides, Mater. Des., 83 (2015) 154-158.

[4] A.C. Kaya, C. Fleck, Deformation behavior of open-cell stainless steel foams, Mater. Sci. Eng. A, 615 (2014) 447-456.

[5] P. Quadbeck, K. Kummel, R. Hauser, G. Standke, J. Adler, G. Stephani, B. Kieback, Structural and material design of open-cell powder metallurgical foams, Adv. Eng. Mater., 13 (2011) 1024-1030.

[6] D.T. Queheillalt, Y. Katsumura, H.N.G. Wadley, Synthesis of stochastic open cell Ni-based foams, Scr. Mater., 50 (2004) 313-317.

[7] R.M. German, A. Bose, Injection Molding of Metals and Ceramics, Metal Powder Industries Federation, 1997.

[8] J.P. Li, C.A. Van Blitterswijk, K. De Groot, Factors having influence on the rheological properties of Ti6A14V slurry, J. Mater. Sci. - Mater. Med., 15 (2004) 951-958.

[9] E. Zaman, O. Keles, Open cell aluminum foams produced by polymer impregnation method, Acta Phys. Pol. A, 125 (2014) 445-448.

[10] C.Y. Zhao, T.J. Lu, H.P. Hodson, J.D. Jackson, The temperature dependence of effective thermal conductivity of open-celled steel alloy foams, Mater. Sci. Eng. A, 367 (2004) 123-131.

[11] J.P. Li, S.H. Li, C.A. Van Blitterswijk, K. de Groot, A novel porous Ti6Al4V: characterization and cell attachment, J. Biomed. Mater. Res. Part A, 73A (2005) 223-233.

[12] P. Quadbeck, J. Kaschta, R.F. Singer, Superalloy IN625 with cellular microstructure - Fabrication route and mechanical properties, Adv. Eng. Mater., 6 (2004) 635-639.

[13] D.T. Queheillalt, D.D. Hass, D.J. Sypeck, H.N.G. Wadley, Synthesis of open-cell metal foams by templated directed vapor deposition, J. Mater. Res., 16 (2001) 1028-1036.

[14] P. Li, Constitutive and failure behaviour in selective laser melted stainless steel for microlattice structures, Mater. Sci. Eng. A, 622 (2015) 114-120.

[15] P. Li, N. Petrinic, C.R. Siviour, Microstructure and x-ray microtomographic characterisation of deformation in electrodeposited nickel thin-walled hollow spheres, Mater. Lett., 100 (2013) 233-236.

[16] Z. Liu, P. Li, N. Srikanth, T. Liu, G.B. Chai, Quantification of flexural fatigue life and 3D damage in carbon fibre reinforced polymer laminates, Compos. Part A, 90 (2016) 778-785.

[17] R. Huang, P. Li, Z.Y. Wang, T. Liu, X-ray microtomographic characterization and quantification of the strain rate dependent failure mechanism in cenosphere epoxy syntactic foams, Adv. Eng. Mater., 18 (2016) 1550-1555.

[18] P. Li, N.V. Nguyen, H. Hao, Dynamic compressive behaviour of Mg foams manufactured by the direct foaming process, Mater. Des., 89 (2016) 636-641.

[19] M.F. Ashby, A.G. Evans, N.A. Fleck, L.J. Gibson, J.W. Hutchinson, H.N.G. Wadley, Metal Foams: A Design Guide, Butterworth-Heinemann, 2000.

[20] F.S. Han, G. Seiffert, Y.Y. Zhao, B. Gibbs, Acoustic absorption behaviour of an open-celled aluminium foam, J. Phys. D-Appl. Phys., 36 (2003) 294-302.

[21] T.J. Lu, F. Chen, D.P. He, Sound absorption of cellular metals with semiopen cells, J. Acoust. Soc. Am., 108 (2000) 1697-1709.

[22] T.J. Lu, A. Hess, M.F. Ashby, Sound absorption in metallic foams, J. Appl. Phys., 85 (1999) 7528-7539.

[23] Z.X. Lu, Q. Liu, J.X. Huang, Analysis of defects on the compressive behaviors of open-cell metal foams through models using the FEM, Mater. Sci. Eng. A, 530 (2011) 285-296.

[24] F. Campana, E. Mancini, D. Pilone, M. Sasso, Strain rate and density-dependent strength of AlSi7 alloy foams, Mater. Sci. Eng. A, 651 (2016) 657-667.

[25] P. Li, Z. Wang, N. Petrinic, C.R. Siviour, Deformation behaviour of stainless steel microlattice structures by selective laser melting, Mater. Sci. Eng. A, 614 (2014) 116-121.

[26] W.Y. Jang, A.M. Kraynik, S. Kyriakides, On the microstructure of open-cell foams and its effect on elastic properties, Int. J. Solids Struct., 45 (2008) 1845-1875.

[27] M.F. Ashby, The properties of foams and lattices, Philos. Trans. R. Soc. A, 364 (2006) 15-30.

[28] H. Choe, D.C. Dunand, Mechanical properties of oxidation-resistant Ni-Cr foams, Mater. Sci. Eng. A, 384 (2004) 184-193.

List of Tables

Table 1 The composition of three types of Inconel 625 slurries.

Inconel 625 powder (g)	PVB (g)	Stearic acid (g)	Ethanol (g)	Slurry Solid loading, Φ
54	1.75	0.80	8.0	0.72
66	1.75	0.80	8.0	0.76
84	1.75	0.80	8.0	0.80

Table 2 The effect of slurry composition on the physical and mechanical properties of open-cell Inconel 625 foams manufactured by the slurry coating method.

Slurry solid loading, Φ	Physical and mechanical properties of the foams			
	Bulk density, ρ (kg m^{-3})	Young's modulus, E (MPa)	Peak stress, σ_{pk} (MPa)	Plateau stress, σ_{pl} (MPa)
0.72	291±25	72±8	1.23±0.20	0.59±0.06
0.76	429±20	146±13	2.63±0.29	1.17±0.11
0.80	720±55	240±35	4.51±0.85	2.59±0.15

List of Figures

Fig. 11 Sound absorption coefficient as a function of frequency for two Inconel foams with different unit cell sizes.

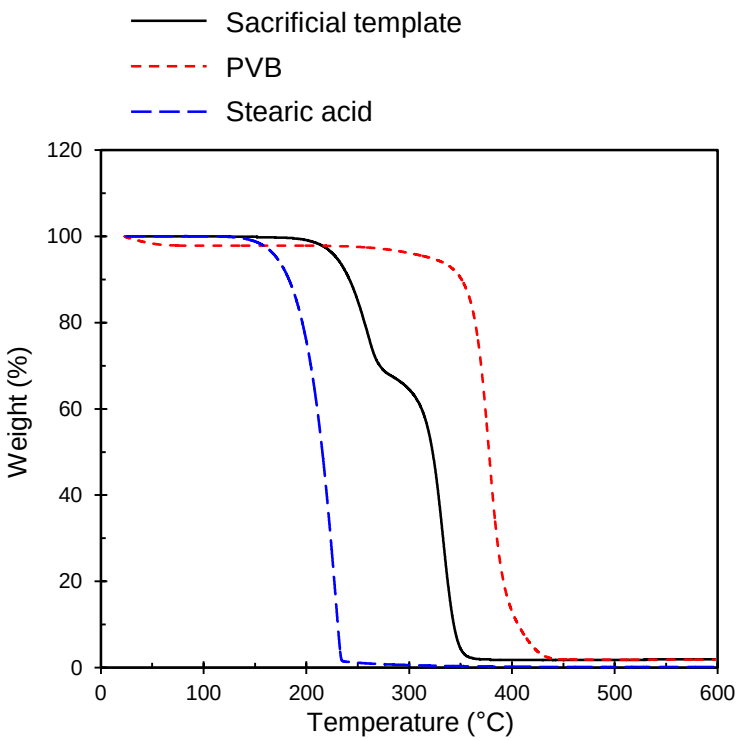

Figure 1: Thermogravimetric analysis (TGA) curves of the sacrificial template, polyvinyl butyral (PVB) and stearic acid. Note that the PVB binder and stearic acid dispersant are two of the components in the slurry.

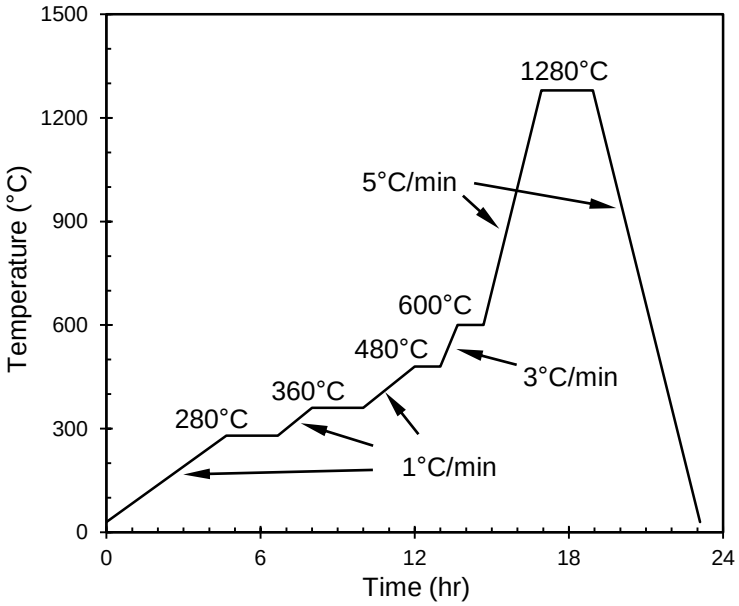

Figure 2: Thermal profile during the sintering process of open-cell Inconel 625 foams.

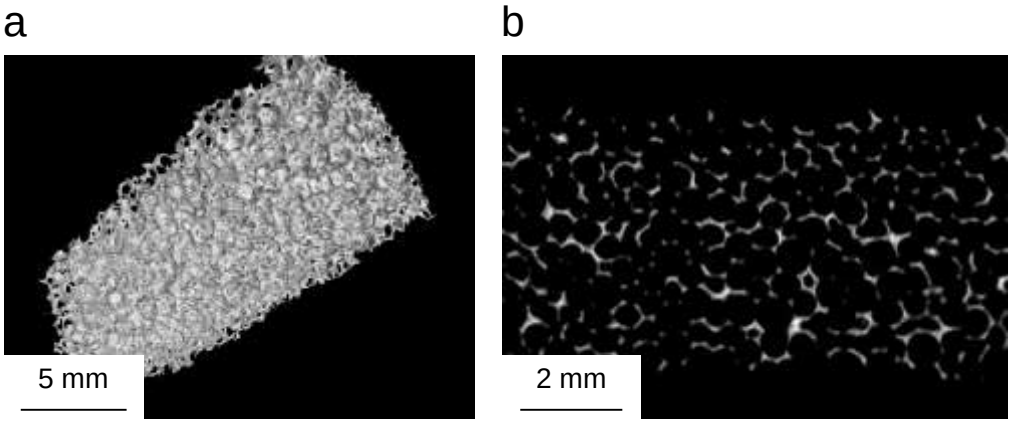

Figure 3: X-ray microtomographic images of open-cell Inconel foams manufactured by the slurry coating technique: (a) 3D view and (b) 2D slice. Note that the solid loading of the slurry is $\Phi = 0.76$.

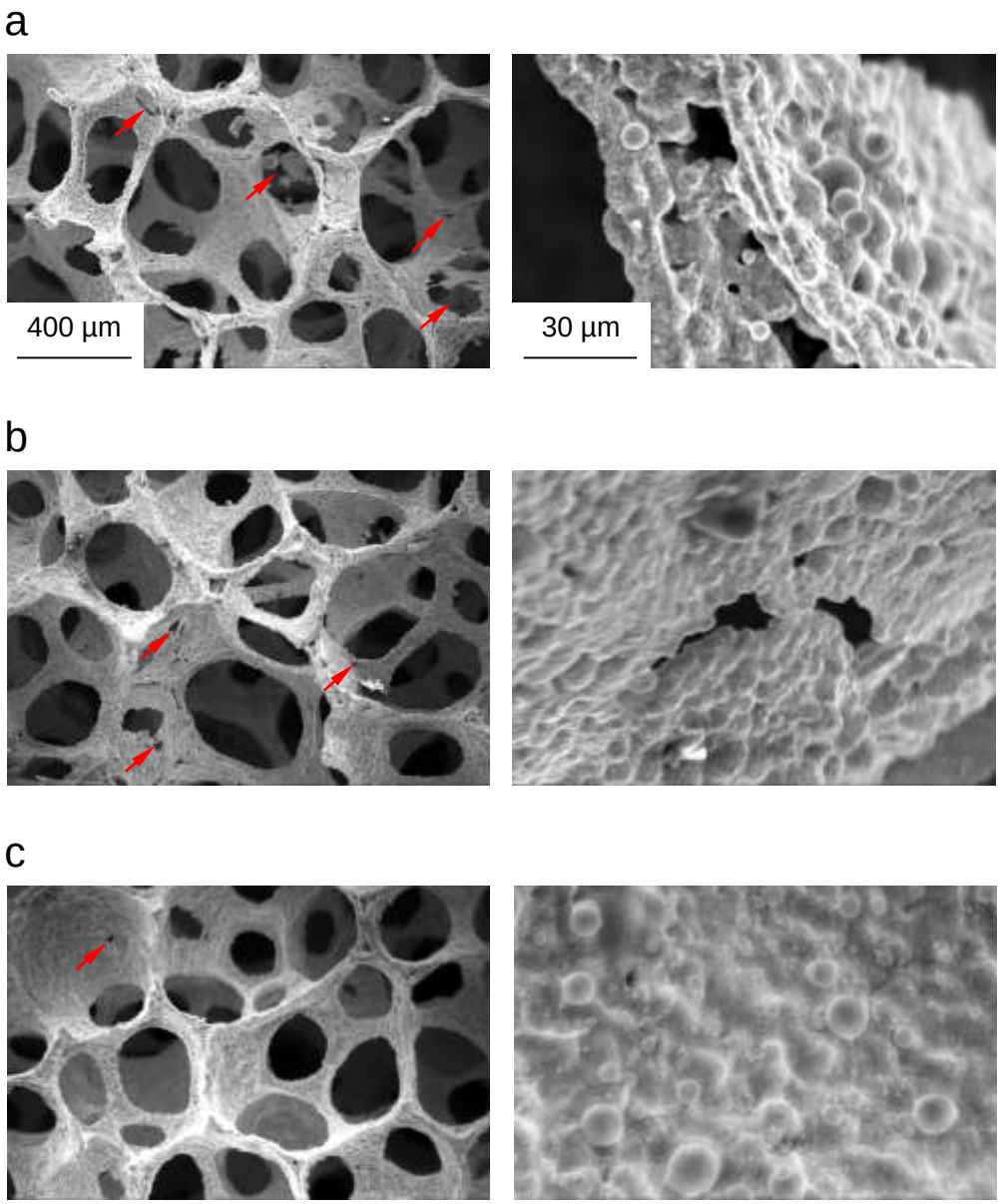

Figure 4: SEM images of the microstructure in open-cell Inconel foams sintered from the slurries with different solid loadings: (a) Φ = 0.72, (b) Φ = 0.76 and (c) Φ = 0.80. Typical micro-pores in strut walls are indicated by the arrows and also shown in the right figures. Note that the scale bars as indicated in (a) apply to the SEM images in (b) and (c).

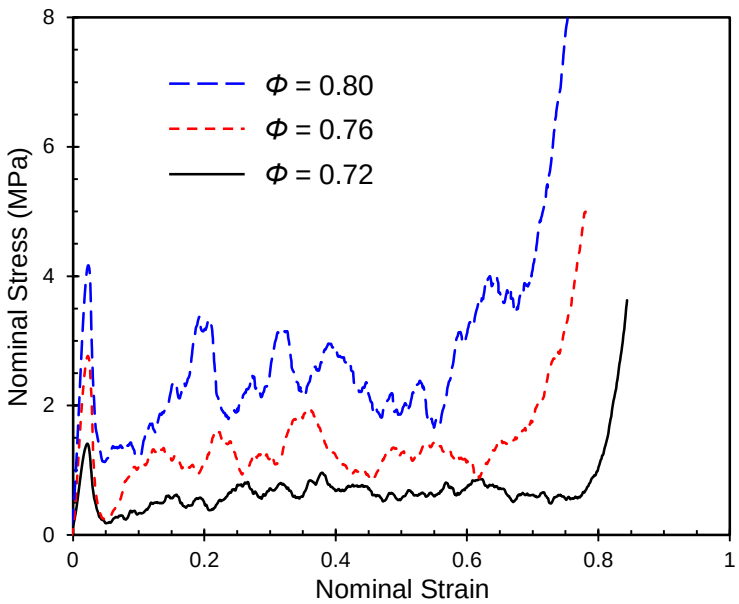

Figure 5: The typical stress–strain curves of open-cell Inconel foams as a function of the solid loading of slurries.

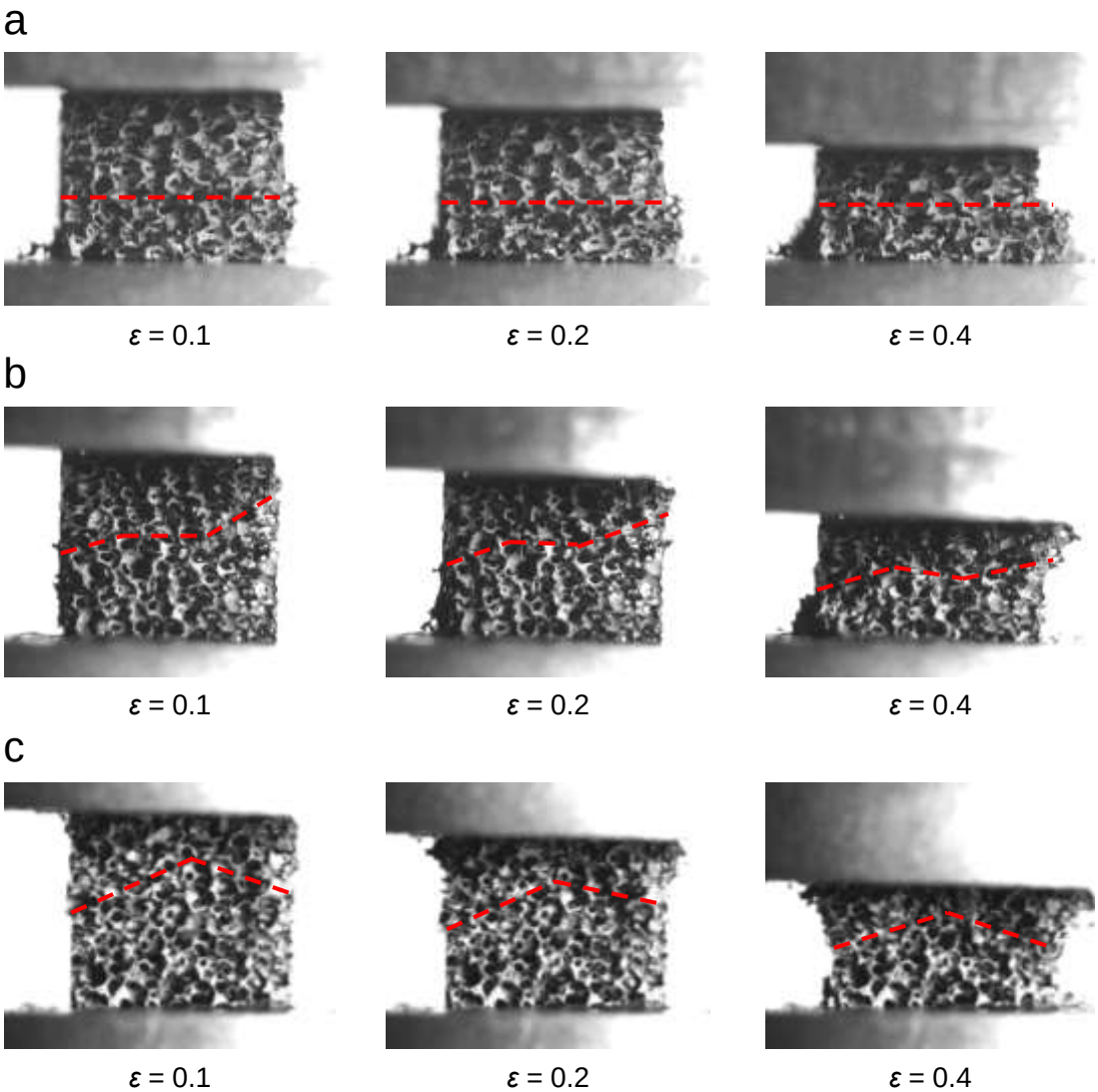

Figure 6: Deformation history of open-cell Inconel foams sintered from the slurries with different solid loadings: (a) $\Phi = 0.72$, (b) $\Phi = 0.76$ and (c) $\Phi = 0.80$. Crush bands are indicated by the dashed lines.

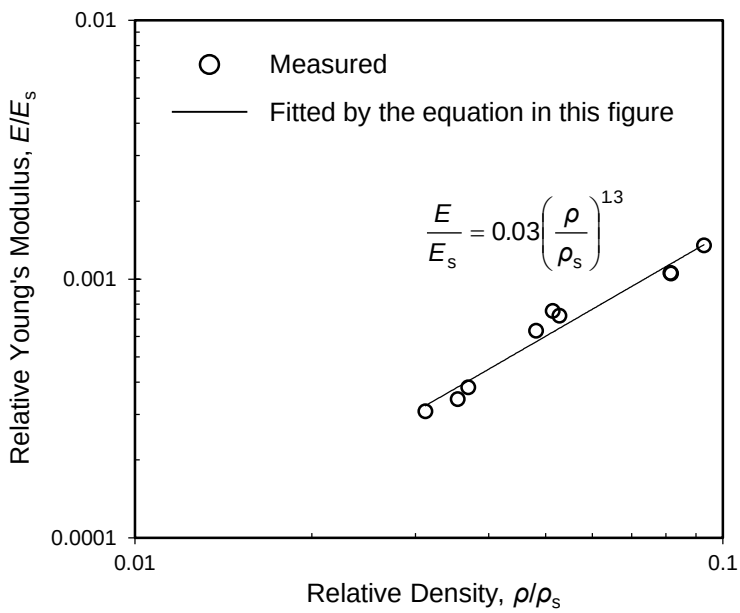

Figure 7: Variation of relative Young's modulus with the relative density of Inconel foams.

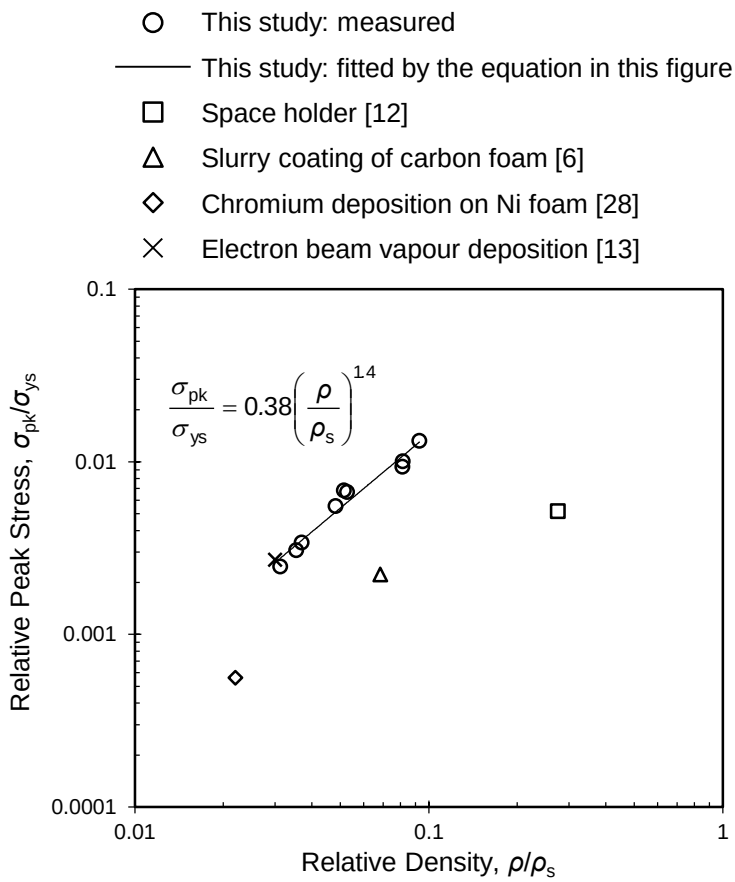

Figure 8: Variation of relative peak stress with the relative density of Inconel foams, and comparison to the data of Ni-based foams made by different fabrication techniques.

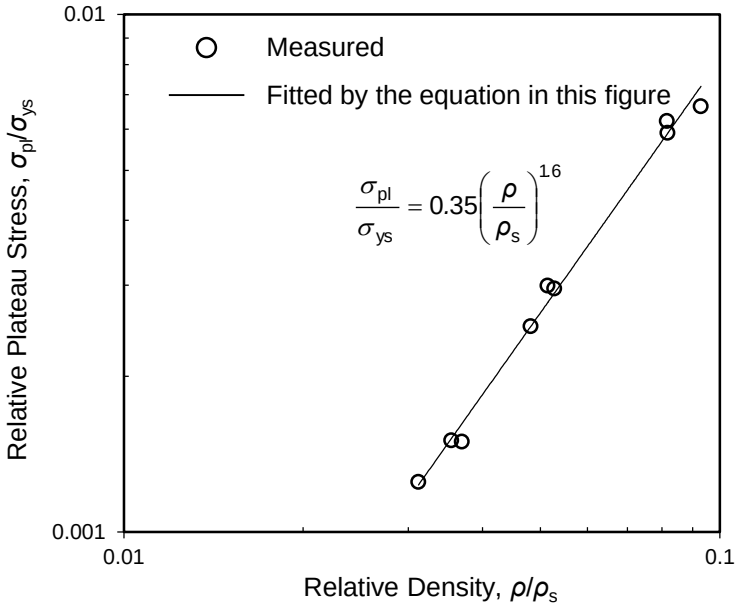

Figure 9: Variation of relative plateau stress with the relative density of Inconel foams.

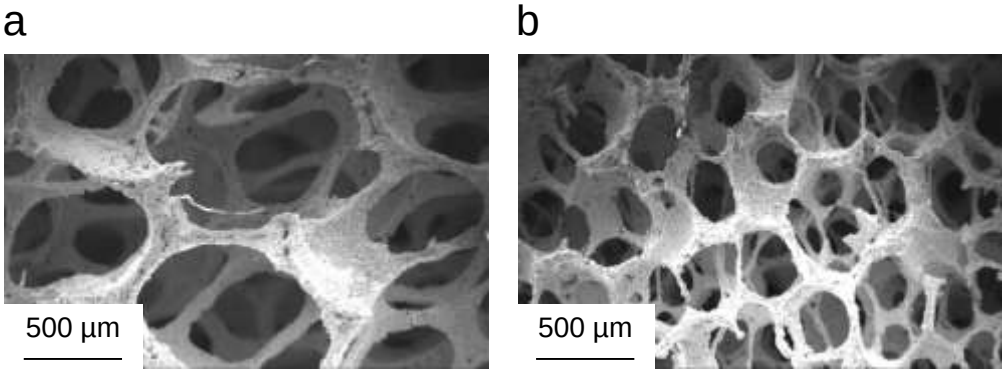

Figure 10: SEM images of the microstructure in open-cell Inconel foams with the unit cell sizes (a) 508–635 µm and (b) 282–339 µm for acoustic testing, which were fabricated from the Regicell 45 and Regicell 80 polyester foam templates, respectively.

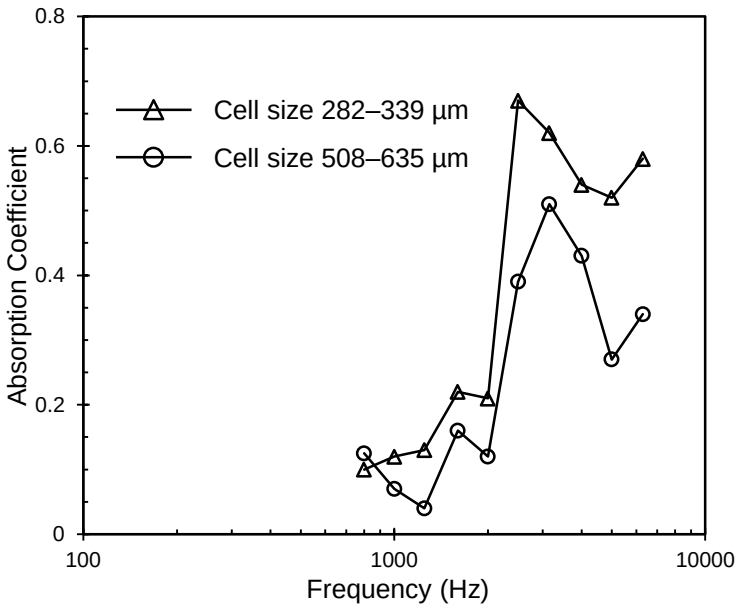

Figure 11: Sound absorption coefficient as a function of frequency for two Inconel foams with different unit cell sizes.